Mass transfer and gas-liquid interface properties of single CO_2 bubbles rising in tap water

W.J. Nock, S. Heaven, C.J. Banks

Chemical Engineering Science

www.elsevier.com/locate/ces

PII: S0009-2509(15)00663-6
DOI: http://dx.doi.org/10.1016/j.ces.2015.10.001
Reference: CES12618

To appear in: *Chemical Engineering Science*

Received date: 13 July 2015
Revised date: 25 September 2015
Accepted date: 4 October 2015

Cite this article as: W.J. Nock, S. Heaven and C.J. Banks, Mass transfer and gas liquid interface properties of single CO_2 bubbles rising in tap water, *Chemica Engineering Science,* http://dx.doi.org/10.1016/j.ces.2015.10.001

Mass transfer and gas-liquid interface properties of single CO_2 bubbles rising in tap water

W.J. Nock*, S. Heaven*, C.J. Banks*

Faculty of Engineering and the Environment, University of Southampton, Highfield, Southampton, SO17 1BJ, United Kingdom

Abstract

To improve the mass transfer efficiency in many industrial applications better understanding of the mass transfer rate is required. High speed images of single CO_2 bubbles rising in tap water were analysed to investigate the relationship between the mass transfer and properties of single bubbles. Transition to a lower mass transfer rate was shown to correspond with the transition from a mobile to an immobile bubble surface. This was indicated by the change in bubble rise velocity, bubble rise path and bubble shape. The presence of surfactants in untreated tap water appear to effect the transition point, particularly for bubbles with a smaller initial diameter and lower rise velocity.

Keywords: mass transfer, bubble, mobile surface, immobile surface, carbon dioxide

1. Introduction

Mass transfer from the gas to the liquid phase is an important process in many industries, including wastewater treatment and aerobic fermentations. It is estimated that 25 % of all reactions in the chemical industry take place in multiphase gas-liquid flows, Martín et al. (2011).

*+44 (0)23 8059 5000
Email address: w.j.nock@soton.ac.uk (W.J. Nock)

The efficiency of the mass transfer process depends on the interfacial area (α) and the properties of the gas-liquid interface. For gases that have a low solubility in the liquid phase, such as CO_2 in water, the gas side mass transfer resistance can be assumed to be negligible, in which case the mass transfer rate ($\frac{dn}{dt}$) can be described by equation 1. Where k_L is the localised liquid side mass transfer coefficient, c^* is the saturated concentration at equilibrium with the partial pressure of the gas, which can be approximated from Henry's law and c_L is the dissolved concentration of the solute.

$$\frac{dn}{dt} = k_L \alpha \left(c^* - c_L\right) \tag{1}$$

The mass transfer coefficient can be represented in dimensionless form by the Sherwood number (Sh), shown in equation 2. In this case d_e is the bubble diameter and D_L is liquid diffusivity of the dissolving gas. When scaling up single bubble experiments it is important to consider the effects of neighbouring bubbles within the bubble swarm and effect this has on bubble properties and mass transfer rate. Apart from the number of bubbles involved, the bubble dimensions and fluid properties from experiments in this work of a single bubble rising through water will be the same for a full scale process.

$$Sh = \frac{k_L d_e}{D_L} \tag{2}$$

Previously there have been many attempts to approximate the mass transfer coefficient for single bubbles and bubble column reactors, with reviews provided by Shah et al. (1982); Kulkarni (2007); Perry and Green (2008). In practice the mass transfer coefficient can be divided between two approaches; for an immobile and mobile gas-liquid interface. Frössling (1938) derived equation 3 using a boundary analysis for a solid sphere, which provides a good approximation for an immobile gas-liquid interface. The terms in equation 3 include u_b the bubble rise velocity and ν_L the dynamic viscosity of the liquid phase. Values for the

coefficient c from equation 3 range from 0.42 - 0.95, Griffith (1960); Lochiel and Calderbank (1964).

$$k_L = c\sqrt{\frac{u_b}{d_e}} D_L^{(2/3)} \nu_L^{(-1/6)} \tag{3}$$

In dimensionless form Frösslings equation is shown in equation 4 using the Reynolds (Re) and Schmidt numbers (Sc), defined by equations 5 and 6, respectively. The liquid density is represented by ρ_L and the liquid dynamic viscosity by μ_L. Typically values for the coefficient b in equation 4 range from 0.5 - 0.6, Perry and Green (2008).

$$Sh = 2 + bRe^{1/2}Sc^{1/3} \tag{4}$$

$$Re = \frac{d_e u_b \rho_L}{\mu_L} \tag{5}$$

$$Sc = \frac{\mu}{\rho_L D_L} \tag{6}$$

Rather than assuming steady state diffusion across the interface Higbie (1935) proposed that the mass transfer coefficient is linked to the time of exposure between the bubble surface and elements of the liquid phase. Using the length of the bubble (or bubble diameter) and the bubble rise velocity as an estimate of the exposure time the mass transfer coefficient can be represented according to Higbies theory by equation 7. The dimensionless form of Higbie's equation is shown in equation 8.

$$k_L = 2\sqrt{\frac{D_L u_b}{\pi d_e}} \tag{7}$$

$$Sh = 1.13Re^{1/2}Sc^{1/2} \tag{8}$$

Leonard and Houghton (1963); Calderbank and Lochiel (1964); Garbarini and Tien (1969) noticed the mass transfer rate from a bubble rising in either tap water or distilled water changed with time. Further experiments to investigate this change in mass transfer have been undertaken with single bubbles held stationary by a downflow of water, Schulze and Schlünder (1985a,b); Vasconcelos et al. (2002, 2003); Alves et al. (2004, 2005). From these experiments a sharp transition in mass transfer rates was detected for a variety of different gases absorbing from single bubbles. The initial mass transfer rate was measured as $3-5$ times larger than the latter rate, Vasconcelos et al. (2002). In such cases Higbies theory can be used to approximate the mass transfer coefficient for the initial part of the bubble rise, where the mass transfer is better approximated by a mobile gas-liquid interface, while Frösslings equation can be used for the latter, where an immobile gas-liquid interface provides a better approximation, Alves et al. (2005).

Surfactants in the liquid phase are recognised to play a role in effecting the gas-liquid interface and mass transfer from bubbles. Surfactants act to reduce the surface tension. Upon attachment onto a bubble the surface flow around the bubble will redistribute the surfactants towards the base of the bubble, resulting in a surface tension gradient and Marangoni effect. The Marangoni force is strong enough to oppose the surface flow, which causes the bubble surface to behave as a rigid interface, Harper et al. (1967).

Although surfactants have a significant effect on bubble properties and the mass transfer rate, the relationship between the bubble surface and accumulation of surfactants is not that well understood. Surfactants can reduce the internal circulation within a bubble, which increases the drag force and reduces the rise velocity. Figure 1 shows two distinct curves for the rise velocity for air bubbles in water. The two curves are based on Maneri and Vassallo (2000) for a mobile bubble surface (un-contaminated by surfactants) and Fan and Tsuchiya (1990) for an immobile bubble surface (contaminated by surfactants). Clift, R., Grace, J.R., Weber (1978) define the spherical, ellipsoidal and spherical cap regimes, of

which the spherical and ellipsodal regimes are considered in this work and shown in figure 1. The bubble regime can also be recognised by the wake structure and rise path, ellipsoidal bubbles can rise either in a helical or zig-zag path, whereas spherical bubbles rise in a rectilinear path.

As can be seen by the correlations proposed by Frössling (1938) and Higbie (1935) in equations 3 and 7, respectively; a higher bubble rise velocity increases k_L. The effect of a lower k_L on total mass transfer will be compensated to some degree by the increased bubble residence time for slower rising bubbles.

Painmanakul et al. (2005) also showed that surfactants can effect the bubble generation process. Conversely the bubble generation process can also effect the bubble rise properties and accumulation of surfactants. This was demonstrated by Peters and Els (2012) who produced both slow and fast moving bubbles using different bubble injection procedures in untreated tap water. Martín et al. (2007) also noted that the bubble generation process is important in determining the bubble rise path oscillations.

The correlations for k_L used in the design of mass transfer systems show wide variability due to the differences between the mobile and immobile bubble surface. This work looks to build on the stationary bubble experiments conducted by Schulze and Schlünder (1985a) and Vasconcelos et al. (2002), by comparing the rise velocity and path oscillations with the mass transfer rate. This work focuses on the absorption of CO_2, as it shows a distinguished transition between mobile and immobile bubble surfaces, Schulze and Schlünder (1985a). Untreated tap water will be used as the liquid phase, thus the surfactant concentration in the liquid phase is unknown. This will be typical for most of the industrial applications where the mass transfer rate plays a crucial role.

2. Methodology

2.1. Experimental Set-up

A square bubble column constructed from 12.0 mm perspex with dimensions $1.1 \times 0.2 \times 0.2$ m was used in this work; a schematic of the experimental set-up is shown in figure 2. A column of diameter greater than 0.15 m should ensure wall effects are negligible, Shah et al. (1982). The square cross-section provided a flat surface which reduced the distortion of photographs taken through the perspex. Photographs of the bubble were taken at 400 fps using a *Phantom Miro eX-4* high speed camera (*Vision Research*, USA), obtained from the *EPSRC* Instrument Loan Pool. A *Nikkon AF Zoom-Nikkor 24-85 mm f/2.8-4D IF* lens with a minimum focus distance of 0.21 m and a macro focal length range between $35 - 85$ mm was attached to the camera. Additional lighting for the high speed photography was provided by two 650 W halogen lights.

The camera was positioned on a platform which was able to traverse along a vertical track the height of the bubble column in order to photograph the bubble at different axial positions. The camera lift was positioned a distance of 0.3 m from the bubble column. The camera platform was connected to a variable speed motor, which controlled the camera movement. Recorded images from the camera were analysed with a computer in real time to track the bubble position: depending on the relative position of the camera and bubble, the velocity of the camera could be adjusted to follow the rise of the bubble. An LV-MaxSonar sonar sensor (MaxBotix Inc., USA) was placed beneath the camera platform, to detect the vertical position of the camera as it travelled up the vertical track. The rise velocity of the bubble was measured with a combination of the sonar sensor and high speed imaging. Experiments were conducted in untreated tap water from the mains supply in Southampton, UK. The tap water was replenished daily allowed to reach ambient temperature ($\approx 20^oC$) and air was sparged through the water for 30 minutes before each set of experiments to ensure the water was saturated with air. The pH and dissolved

oxygen (DO) content of the water was measured periodically throughout the experiments. The pH was measured using a Jenway 3010 meter (Bibby Scientific Ltd, UK) and a combination glass electrode, calibrated in buffers at pH 7 and 9.2. The DO was measured using a YSI 5000 meter (YSI Inc., USA), the probe zero measurement was checked with a sodium sulphite solution. During experimental runs no significant changes in DO or pH were observed. Saturation concentrations of N_2, O_2 and CO_2 from air were therefore assumed throughout the experiments.

Experiments were conducted with bubbles produced from an orifice of 1.0 mm and 0.35 mm diameter. The CO_2 (BOC, UK) was stored in a gas-impermeable sampling bag and pumped into the column using a peristaltic pump (Watson Marlow, UK). A bubble generation frequency of between 30 - 40 bubbles per minute was used in these experiments.

Gas samples were collected at different heights in the bubble column using an inverted funnel connected to a tube and syringe for short-term storage of the gas samples, as shown in figure 2. Several hundred bubbles were required for each gas sample to be taken. Input and output gas samples were analysed using a Varian Star 3400 CX gas chromatograph (GC), (Varian Ltd, Oxford, UK). The GC was fitted with a Hayesep C column with argon as the carrier gas at a flow of 50 $ml\ min^{-1}$ and a thermal conductivity detector. A 2 mL sample was injected into a gas sampling loop and the concentration was compared with standard gas sample containing 100 % CO_2 (BOC, UK) for calibration. The GC measurements were averaged over five replicates.

2.2. Image Analysis

The images obtained from the high speed camera were analysed using tailored MATLAB software with the Image Analysis Toolbox (Mathworks Inc., USA). Figure 3 shows a flow diagram of the image analysis procedure used in this work. Firstly, the initial bubble pixel position was measured from the first image of the sequence. This was input into the code along with an upper and lower limit

estimate of expected bubble sizes. A background image was then constructed using a morphological dilation of the previous image in the video sequence. This background image was subtracted from the bubble image to remove the background detail. An iterative procedure was used to find the threshold value to convert the image from grayscale (with a pixel value between 0 - 255) to a black and white image (with a pixel value of either 0 or 1). Once an initial estimation of the black pixels which represent the bubble edge was made, an iteration to obtain the threshold value was undertaken which maximised the ratio between the number of black pixels in the area of the image where the bubble position was estimated, and the number of pixels in the remainder of the image. The detected bubble segments were then analysed based on their size and position. If these corresponded with the defined bubble size and position the co-ordinates were saved as part of the bubble co-ordinates.

A correction was then applied to the bubble co-ordinates to account for differences in refractive index of the water and perspex, as well as lens distortion from the camera. Following this an algebraic ellipse fitting routine, developed by Gander et al. (1994), was applied to provide an estimate for the minor and major bubble diameter. Figure 4a shows an example of a cropped grayscale image; the black and white conversion with the background removed is shown in figure 4b. The traced bubble segments and fitted ellipse are shown in figure 4c and 4d, respectively.

A test of the image analysis procedure was conducted with a plastic bead of 5.0 mm diameter, which was recorded falling through the water. The average measured bead diameter provided a slight underestimate to the actual diameter, as shown in figure 5.

As observed in the work of Schulze and Schlünder (1985a), Schulze and Schlünder (1985b) and Vasconcelos et al. (2002) mass transfer from the same gas bubble into a liquid can occur at different rates. These authors observed a sharp and prominent transition point between different mass transfer rates. As a result of this, the change in bubble diameter can be approximated by two lines of best

fit. These were calculated using a minimisation of squares approach, which is shown in Appendix A.

2.3. Mass Transfer Rate

The number of moles of gaseous CO_2 in the bubble were calculated for each image assuming the ideal gas law and taking into consideration the change in gas pressure in the bubble at different heights in the water column. This is shown in equation 9 where y_i is the mole fraction of the component i in the gas phase at time j. The components considered in this work were CO_2, and O_2 and N_2 from the air. Equation 9 gives the number of moles of component i at timestep j as n_{ij}, where the atmospheric pressure is p_{atm}, the liquid density is ρ_L, the gravitational constant is g, the bubble volume is v_B, the ideal gas constant is R and the temperature is T. This was combined with interpolated values from the GC from gas samples collected at different heights in the bubble column. The mass transfer rate can then be calculated from the change in number of moles for each component throughout the bubble rise.

$$n_{i,j} = \frac{y_{i,j}\left(p_{atm} + \rho_L g z_j\right) v_{B,j}}{RT} \tag{9}$$

3. Results & Discussion

The effect of the initial bubble diameter on the mass transfer rate for two CO_2 bubbles can be seen in figure 6. The bubble with a larger initial diameter (bubble 'A', $d_0 \approx 2.9\ mm$) in figure 6a shows an approximately constant mass transfer rate, as can be seen by the linear reduction in diameter over time and from k_L in figure 6e. The bubble diameter measurements from the high speed camera images contain a significant degree of noise, part of this is due to the measurement accuracy and part is due to the three-dimensional movement of the bubble as it rises up the column. This horizontal movement can be clearly seen with bubble 'A' which exhibits an oscillation in the bubble diameter due

to the helical rise path, this can occur with bubbles in the ellipsoidal regime. The bubble with a smaller initial diameter (bubble 'B', $d_0 \approx 2.3\ mm$) in figure 6b displays two distinct mass transfer rates, with a higher initial mass transfer rate followed by a reduced value, this is shown by the reduction in the gradient of the bubble diameter over time and from the reduction in k_L in figure 6f. The observation of two distinct mass transfer rates supports the findings of Schulze and Schlünder (1985a) and Vasconcelos et al. (2002) who found that the point at which the transition between the larger and smaller mass transfer rates occurs is dependent on the initial bubble diameter.

The bubble rise velocities and Re for bubble 'A' and 'B' are shown in figures 6c and 6d, respectively. The rise velocity of bubble 'A' shows a more gradual increase than bubble 'B'. Neither bubble 'A' nor bubble 'B' attain a rise velocity over 0.3 $m\ s^{-1}$, which suggests they maybe between the mobile and immobile case. The mass transfer coefficient of bubble 'A' and the initial mass transfer coefficient of bubble 'B' in figures 6e and 6f show $k_L \approx 4.3 - 4.6\ \times\ 10^{-4}\ m\ s^{-1}$ and can be approximated by Higbies theory. The mass transfer coefficient of bubble 'B' undergoes a distinct change, with the latter value of k_L approximated well by Frössling's theory.

The effects of the initial bubble rise velocity on the overall mass transfer rate were compared by producing bubbles from 1.0 mm and 0.35 mm orifices. These bubbles were produced with the same gas flow rate, thus the bubbles from the 0.35 mm orifice had a higher gas velocity than those produced from the 1.0 mm orifice. Figures 7a and 7b compare sequential images at intervals of 0.025 s of the initial rise of two CO_2 bubbles with approximately the same initial bubble diameter ($d_0 \approx 2.7 - 2.8\ mm$). As can be seen by comparing the distances travelled in figures 7a and 7b, after 0.35 s bubble 'D' (from the 0.35 mm orifice) has a higher initial velocity than bubble 'C' (from the 1.0 mm orifice). The two-dimensional oscillation of the bubble path for bubble 'C' and 'D' are shown in figures 7c and 7d. The bubble rise path shows the oscillation of bubble 'C', which is a characteristic of the ellipsoidal bubble regime. The rise path of

bubble 'D' shows an initial oscillation, however this changes to a recti-linear rise path as a result of the transition from the ellipsoidal to the spherical bubble regime.

The higher initial rise velocity of bubble 'D' is not sustained throughout the bubble rise, as shown in figure 8c and 8d. Despite a lower initial velocity bubble 'C' eventually reaches a maximum rise velocity of $u_b \approx 0.3\ m\ s^{-1}$, larger than bubble 'D', which reached a maximum rise velocity of $u_b \approx 0.25\ m\ s^{-1}$. The lower initial rise velocity of bubble 'C' results in a lower initial mass transfer rate, shown by the lower value of k_L in figure 8e. This mass transfer rate increases throughout the bubble rise. Conversely, the higher initial rise velocity of bubble 'D' results in a greater initial mass transfer rate, shown by the higher value of k_L in figure 8f, and thus a greater reduction in bubble volume. This reduction in bubble size results in the earlier onset of the immobile bubble surface, which is not seen for bubble 'C'. This shows that as well as the initial bubble diameter, as recognised by Schulze and Schlünder (1985a) and Vasconcelos et al. (2002), the initial rise velocity also plays a role in defining the transition to the immobile bubble surface.

Bubbles 'A' and 'C' from figures 6 and 8, respectively approach the transition to the immobile bubble surface, with $Re \approx 400$, at the top of the column. The transition point between the mobile and immobile bubble surface is also dependent on surfactant attachment to the bubble. Spherical and ellipsoidal bubbles which are contaminated with surfactants are recognised to have an immobile surface when $Re \approx 200$, Clift, R., Grace, J.R., Weber (1978). Figure 9 shows the effect of the initial bubble diameter and rise velocity on the transition values of Re. Bubbles with an initial bubble diameter ($d_0 > 3.0\ mm$) showed a higher initial rise velocity ($u_0 > 0.25\ m\ s^{-1}$) and the transition to the immobile surface occurred with $400 < Re_T < 600$. Bubbles with a smaller initial diameter ($d_0 \approx 2.4\ mm$) and smaller rise velocity ($u_0 < 0.25\ m\ s^{-1}$) showed a wider range of Re for the transition to the immobile bubble surface, with $200 < Re_T < 600$. Smaller bubbles with a lower rise velocity have been shown to

be more susceptible to the effects of surfactants. Work by Rosso et al. (2006) confirmed that a higher interfacial velocity reduced the effect of surfactants. The interfacial velocity is related to the bubble rise velocity, which is generally higher for larger bubbles. Hence a larger bubble, with a greater velocity, would inhibit the attachment of surfactants to a greater degree than a smaller bubble with a lower rise velocity. This is a possible explanation for the lower values of Reynolds numbers for the transition to an immobile surface for smaller and slower bubbles.

4. Conclusion

Two distinct mass transfer rates were observed in CO_2 bubbles rising in untreated tap water. These were successfully approximated by mass transfer relations for mobile and immobile gas-liquid interfaces. In addition to the initial bubble diameter, the initial rise velocity was shown to effect the mass transfer rate and the transition to the immobile bubble surface. The effect of surfactants appears to have a greater influence on smaller, slower rising bubbles, which can reduce the value of the transition Re, resulting in an earlier onset of the immobile bubble surface and reduced k_L.

5. Acknowledgements

The authors acknowledge the doctoral research grant provided by the Engineering and Physical Sciences Research Council (EPSRC) and the use of the Vision Research high speed camera which was borrowed from the EPSRC Engineering Instrument Pool.

Appendix A. Appendix A

Equations A.1 - A.3 represent the minimisation of squares to find the two lines of best fit, while x_{sep} in equation A.4 represents the x value at the intersection

between the first and second linear models.

$$y_1 = \alpha_1 x_1 + \beta_1 \qquad\qquad y_2 = \alpha_2 x_2 + \beta_2 \tag{A.1}$$

$$\alpha_1 = \frac{n_1 \Sigma x_1 y_1 - \Sigma x_1 \Sigma y_1}{n_1 \Sigma x_1^2 - (\Sigma x_1)^2} \qquad\qquad \alpha_2 = \frac{n_2 \Sigma x_2 y_2 - \Sigma x_2 \Sigma y_2}{n_2 \Sigma x_2^2 - (\Sigma x_2)^2} \tag{A.2}$$

$$\beta_1 = \frac{\Sigma x_1^2 \Sigma y_1 - \Sigma x_1 \Sigma x_1 y_1}{n_1 \Sigma x_1^2 - (\Sigma x_1)^2} \qquad\qquad \beta_2 = \frac{\Sigma x_2^2 \Sigma y_2 - \Sigma x_2 \Sigma x_2 y_2}{n_2 \Sigma x_2^2 - (\Sigma x_2)^2} \tag{A.3}$$

$$x_{sep} = \frac{\beta_2 - \beta_1}{\alpha_1 - \alpha_2} \tag{A.4}$$

M. Martín, M. a. Galán, R. L. Cerro, F. J. Montes, Shape oscillating bubbles: hydrodynamics and mass transfer - a review, Bubble Science, Engineering & Technology 3 (2) (2011) 48–63.

Y. Shah, B. Kelkar, S. Godbole, W. Deckwer, Design Parameters Estimations for Bubble Column Reactors, AIChE Journal 28 (3) (1982) 353 – 375.

A. A. Kulkarni, Mass Transfer in Bubble Column Reactors: Effect of Bubble Size Distribution, Industrial & Engineering Chemistry Research 46 (2007) 2205–2211.

R. H. Perry, D. W. Green, Perry's Chemical Engineers' Handbook, McGraw Hill, New York, 8th edn., 2008.

N. Frössling, Über die verdunstung fallender tropfen (On the evaporation of falling drops), Gerlands Beiträge zur Geophysik 52 (1938) 170–215.

R. Griffith, Mass Transfer from drops and bubbles, Transactions of the Institute of Chemical Engineers 12 (3) (1960) 198 – 213.

A. Lochiel, P. Calderbank, Mass transfer in the continuous phase around axisymmetric bodies of revolution, Chemical Engineering Science 19 (1964) 471 – 484.

R. Higbie, The rate of absorption of a pure gas into still liquid during short periods of exposure 31.

J. Leonard, G. Houghton, Mass transfer and velocity of rise phenomena for single bubbles, Chemical Engineering Science 18 (1963) 133 – 142.

P. Calderbank, A. Lochiel, Mass transfer coefficients, velocities and shapes of carbon dioxide bubbles in free rise through distiled water, Chemical Engineering Science 19 (1964) 485 – 503.

G. Garbarini, C. Tien, Mass Transfer from Single Gas Bubble - A Comparative Study on Experimental Methods, The Canadian Journal of Chemical Engineering 47 (1) (1969) 35 – 41.

G. Schulze, E. Schlünder, Physical absorption of single gas bubbles in degassed and preloaded water, Chemical Engineering and Processing: Process Intensification .

G. Schulze, E. Schlünder, The effect of multicomponent diffusion on the mass transfer during absorption of single gas bubbles, Chemical Engineering and Processing: Process Intensification .

J. Vasconcelos, S. Orvalho, S. Alves, Gas-Liquid Mass Transfer to Single Bubbles: Effect of Surface Contamination, AIChE journal 48 (6) (2002) 1145 – 1154.

J. Vasconcelos, J. Rodrigues, S. Orvalho, S. Alves, R. Mendes, A. Reis, Effect of contaminants on mass transfer coefficients in bubble column and airlift contactors, Chemical Engineering Science 58 (8) (2003) 1431–1440.

S. Alves, C. Maia, J. Vasconcelos, Gas-liquid mass transfer coefficient in stirred tanks interpreted through bubble contamination kinetics, Chemical Engineering and Processing 43 (7) (2004) 823–830, ISSN 02552701.

S. S. Alves, S. P. Orvalho, J. M. T. Vasconcelos, Effect of bubble contamination on rise velocity and mass transfer, Chemical Engineering Science 60 (2005) 1–9.

J. F. Harper, D. W. Moore, J. R. A. Pearson, The effect of the variation of surface tension with temperature on the motion of bubbles and drops, Journal of Fluid Mechanics 27 (2) (1967) 361–366.

C. C. Maneri, P. F. Vassallo, Dynamics of Bubbles Rising in Finite and Infinite Media, Tech. Rep., American Institute of Chemical Engineers, 2000.

L.-S. Fan, K. Tsuchiya, Bubble wake dynamics in liquids and liquid-solid dispersions, Butterworth-Heinemann, 1990.

M. Clift, R., Grace, J.R., Weber, Ellipsoidal Fluid Particles, in: Bubbles, Drops and Particles, Academic Press, 169 – 202, 1978.

P. Painmanakul, K. Loubière, G. Hébrard, M. Mietton-Peuchot, M. Roustan, Effect of surfactants on liquid-side mass transfer coefficients, Chemical Engineering Science 60 (22) (2005) 6480–6491.

F. Peters, C. Els, An experimental study on slow and fast bubbles in tap water, Chemical Engineering Science 82 (2012) 194–199.

M. Martín, F. J. Montes, M. a. Galán, Oxygen transfer from growing bubbles: Effect of the physical properties of the liquid, Chemical Engineering Journal 128 (1) (2007) 21–32, ISSN 13858947.

W. Gander, G. H. Golub, R. Strebel, Least-squares fitting of circles and ellipses, Bit Numerical Mathematics 34 (4) (1994) 558–578.

D. Rosso, D. L. Huo, M. K. Stenstrom, Effects of interfacial surfactant contamination on bubble gas transfer, Chemical Engineering Science 61 (2006) 5500–5514.

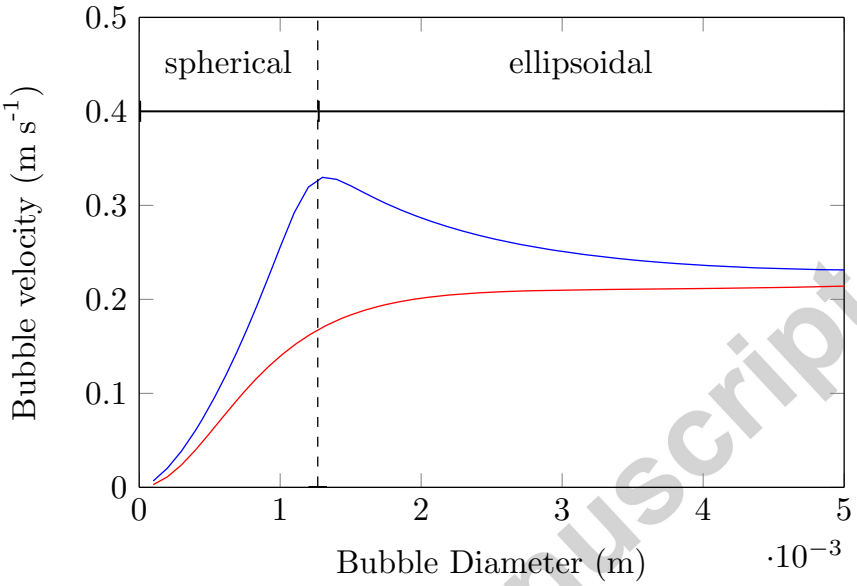

Figure 1: Bubble Rise Velocity

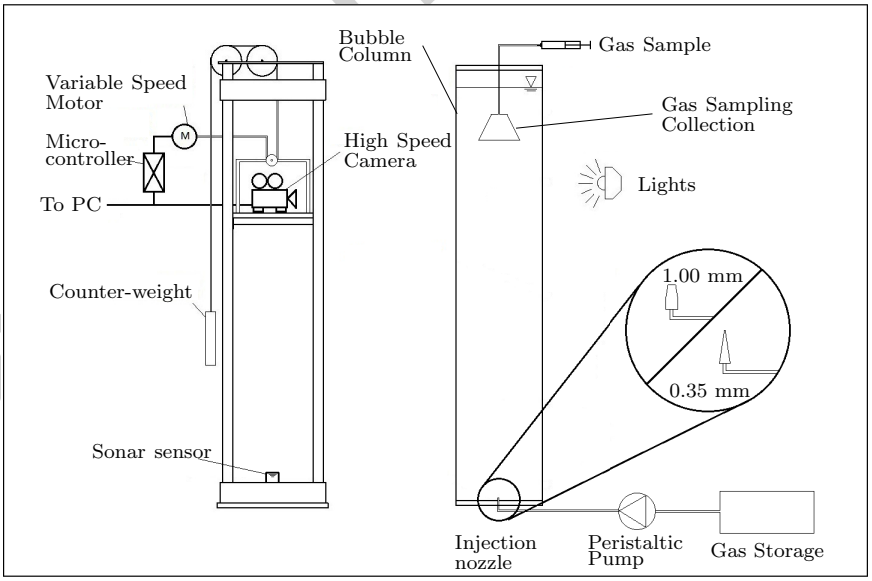

Figure 2: Schematic of single bubble experimental set-up

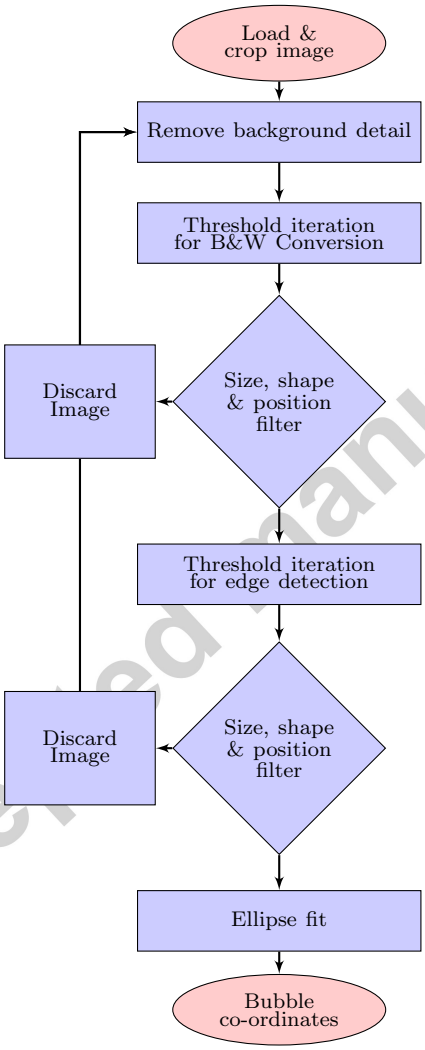

Figure 3: Image Processing Flow Diagram

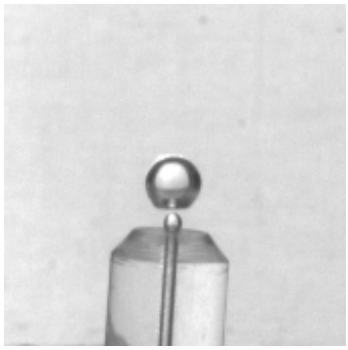

(a) Cropped Image

(b) Binary image with background removed

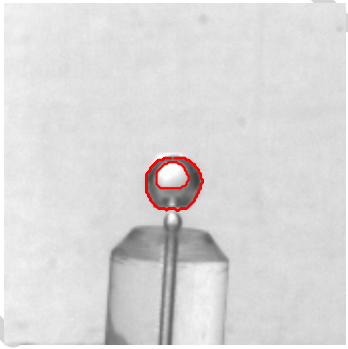

(c) Image with detected edge

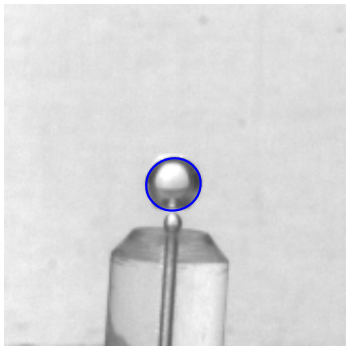

(d) Image with fitted ellipse

Figure 4: Image analysis sequence

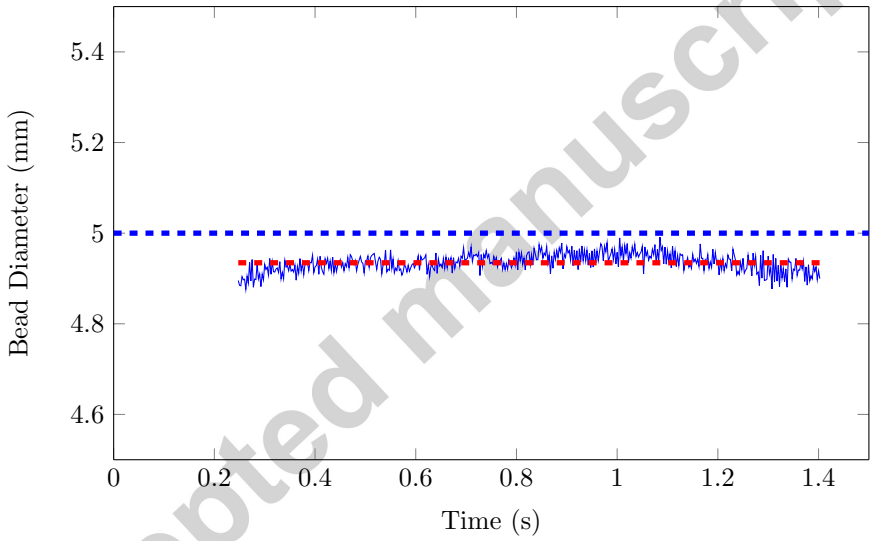

Figure 5: Calibration with 5.0mm diameter bead

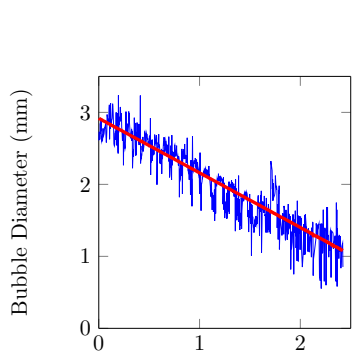

(a) Change in bubble 'A' diameter

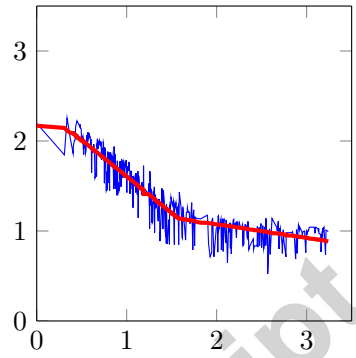

(b) Change in bubble 'B' diameter

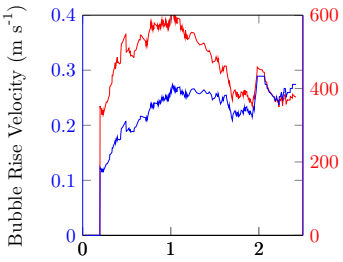

(c) Rise velocity and Re of bubble 'A'

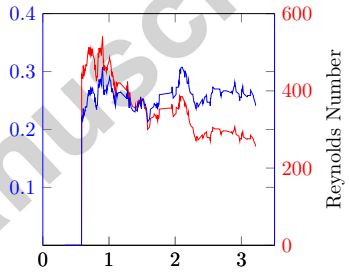

(d) Rise velocity and Re of bubble 'B'

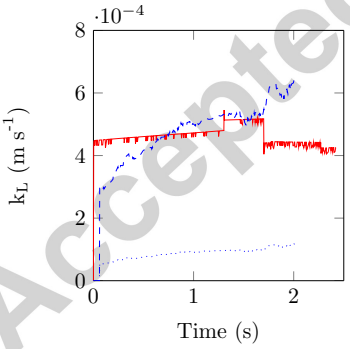

(e) k_L for bubble 'A'

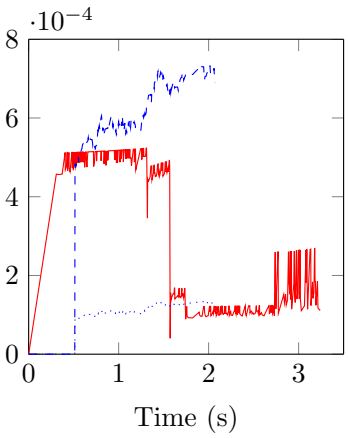

(f) k_L for bubble 'B'

Figure 6: Comparison between the change in bubble diameter, rise velocity and Reynolds number for two pure CO_2 bubbles (bubble 'A' and bubble 'B') with different initial bubble diameters rising in tap water.

(a) Visualisation of initial rise of bubble 'C'. Images shown 0.025 s apart

(b) Visualisation of initial rise of bubble 'D'. Images shown 0.025 s apart

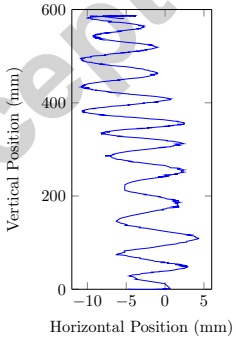

(c) 2D Bubble rise path of bubble 'C'

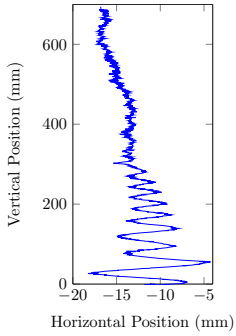

(d) 2D Bubble rise path of bubble 'D'

Figure 7: Comparison of bubble rise path of bubble 'C', with $u_0 \approx 0.2\ m\ s^{-1}$, $d_0 \approx 2.7\ mm$ and bubble 'D' with $u_0 \approx 0.3\ m\ s^{-1}$, $d_0 \approx 2.8\ mm$

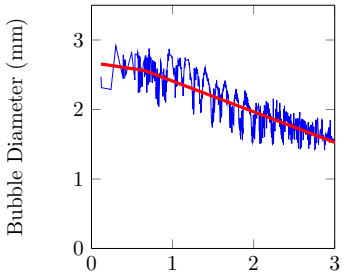

(a) Change in bubble 'C' diameter

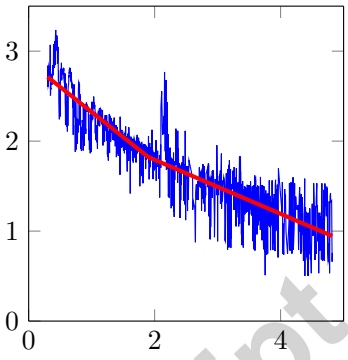

(b) Change in bubble 'D' diameter

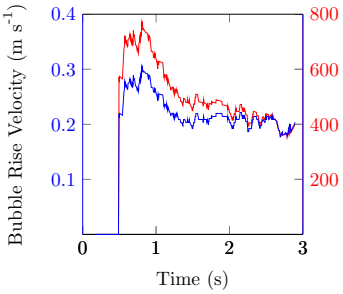

(c) Rise velocity and Re of bubble 'C'

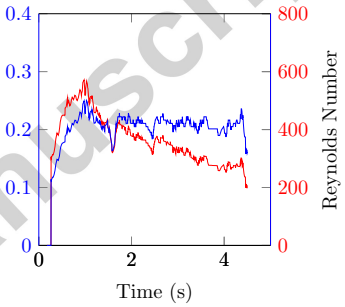

(d) Rise velocity and Re of bubble 'D'

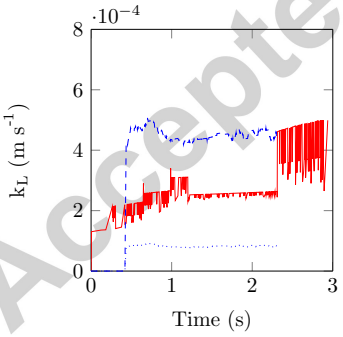

(e) k_L for bubble 'C'

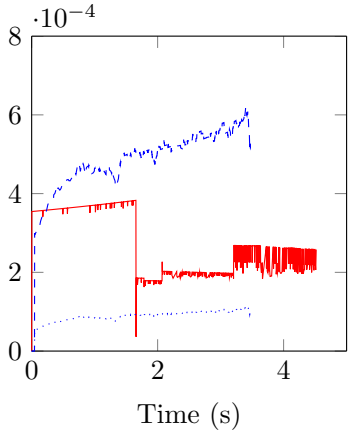

(f) k_L for bubble 'D'

Figure 8: Comparison between the change in bubble diameter, rise velocity and Reynolds number for two pure CO_2 bubbles (bubble 'C' and bubble 'D') with different initial bubble rise velocities rising in tap water.

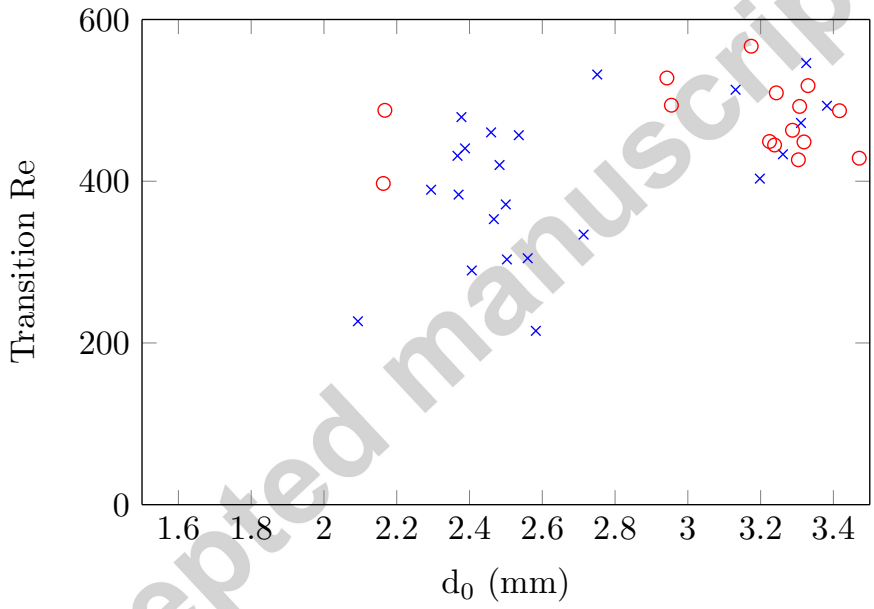

Figure 9: Transition Reynolds number (Re) for bubbles produced from the 1.0 *mm* and 0.35 *mm* orifice